Journal of Volcanology and Geothermal Research 348 (2017) 36–48

Contents lists available at ScienceDirect

Journal of Volcanology and Geothermal Research

journal homepage: www.elsevier.com/locate/jvolgeores

Compositional and volumetric development of a monogenetic lava flow field: The historical case of Paricutin (Michoacán, Mexico)

Patricia Larrea [a,b,*], Sergio Salinas [c], Elisabeth Widom [a], Claus Siebe [d], Robbyn J.F. Abbitt [e]

[a] Department of Geology and Environmental Earth Science, Miami University, Oxford, OH 45056, USA
[b] School of Geological Sciences and Engineering, Yachay Tech, Urcuquí, Imbabura, Ecuador
[c] Facultad de Ingeniería, División de Ingeniería en Ciencias de la Tierra, Universidad Nacional Autónoma de México, Ciudad Universitaria, C.P. 04510 Coyoacán, Ciudad de México, Mexico
[d] Departamento de Vulcanología, Instituto de Geofísica, Universidad Nacional Autónoma de México, Ciudad Universitaria, C.P. 04510 Coyoacán, México D.F., Mexico
[e] Department of Geography, Miami University, Oxford, OH 45056, USA

ARTICLE INFO

Article history:
Received 2 August 2017
Received in revised form 21 October 2017
Accepted 22 October 2017
Available online 23 October 2017

Keywords:
Paricutin volcano
Michoacán–Guanajuato volcanic field
Monogenetic volcanism
Eruptive phase
ArcGIS mapping
Lava field volumetric estimations

ABSTRACT

Paricutin volcano is the youngest and most studied monogenetic volcano in the Michoacán-Guanajuato volcanic field (Mexico), with an excellent historical record of its nine years (February 1943 to March 1952) of eruptive activity. This eruption offered a unique opportunity to observe the birth of a new volcano and document its entire eruption. Geologists surveyed all of the eruptive phases in progress, providing maps depicting the volcano's sequential growth. We have combined all of those previous results and present a new methodological approach, which utilizes state of the art GIS mapping tools to outline and identify the 23 different eruptive phases as originally defined by Luhr and Simkin (1993). Using these detailed lava flow distribution maps, the volume of each of the flows was estimated with the aid of pre- and post-eruption digital elevation models. Our procedure yielded a total lava flow volume ranging between 1.59 and 1.68 km^3 DRE, which is larger than previous estimates based on simpler methods. In addition, compositional data allowed us to estimate magma effusion rates and to determine variations in the relative proportions of the different magma compositions issued during the eruption. These results represent the first comprehensive documentation of the combined chemical, temporal, and volumetric evolution of the Paricutin lava field and provide key constraints for petrological interpretations of the nature of the magmatic plumbing system that fed the eruption.

© 2017 Elsevier B.V. All rights reserved.

1. Introduction

On the order of twenty volcanic eruptions are taking place at any given time around the globe (USGS Weekly Volcanic Activity Report), practically all belonging to stratovolcanoes that have been recurrently active for thousands of years. There have been only few occasions in historical times when scientists had the opportunity to observe the birth of a new volcano and document its entire eruptive cycle. These short-lived volcanoes are known as monogenetic and their eruptions are normally characterized by a small volume of magma produced by a single episode of volcanic activity lasting from several days to years, and forming scoria cones, maars, tuff cones, or lava domes and lava shields (e.g. Connor and Conway, 2000; Németh et al., 2017). Most monogenetic volcanoes are scoria cones, a few examples of which have erupted in historic times, including Waiowa (1943–1944 CE) in Papua New Guinea, Monte Nuovo (1538 CE) in Italy, and Jorullo (1759–1774 CE) and Paricutin (1943–1952 CE) in the Michoacán-Guanajuato volcanic field (MGVF) of Mexico.

The Michoacán-Guanajuato Volcanic Field (MGVF) in the Trans-Mexican Volcanic Belt (TMVB; Fig. 1a) is the largest monogenetic field on Earth (Valentine and Connor, 2015), containing >1000 eruptive centers (Hasenaka and Carmichael, 1985), the majority of which are scoria cones that formed by explosive Strombolian activity interspersed with effusive phases during which lava flows were emitted. Although the exact reasons for the large concentration of monogenetic volcanoes in this volcanic field remain unclear, recent studies point to the unique geometric configuration of the subduction zone as the main feature controlling the location and areal extent of magmatism (e.g. Kim et al., 2012; Chevrel et al., 2016a). The near-horizontal position of the subducting Cocos plate underneath the North American Plate at a depth of 90–120 km might be inducing partial melting of the mantle wedge over this wide area beneath the ~40-km-thick continental crust. Moreover, as pointed out by Guilbaud et al. (2012), the hazard of future monogenetic activity in the MGVF has not yet been effectively assessed, as reliable estimates of emitted magma volumes, effusion rates and eruption recurrence rates are relatively sparse, although some studies have recently been published on MGVF volcanoes such

* Corresponding author at: School of Geological Sciences and Engineering, Yachay Tech, Hacienda San José c/n y Proyecto Yachay, San Miguel de Urcuquí, Ecuador.
E-mail address: larreap@miamioh.edu (P. Larrea).

https://doi.org/10.1016/j.jvolgeores.2017.10.016
0377-0273/© 2017 Elsevier B.V. All rights reserved.

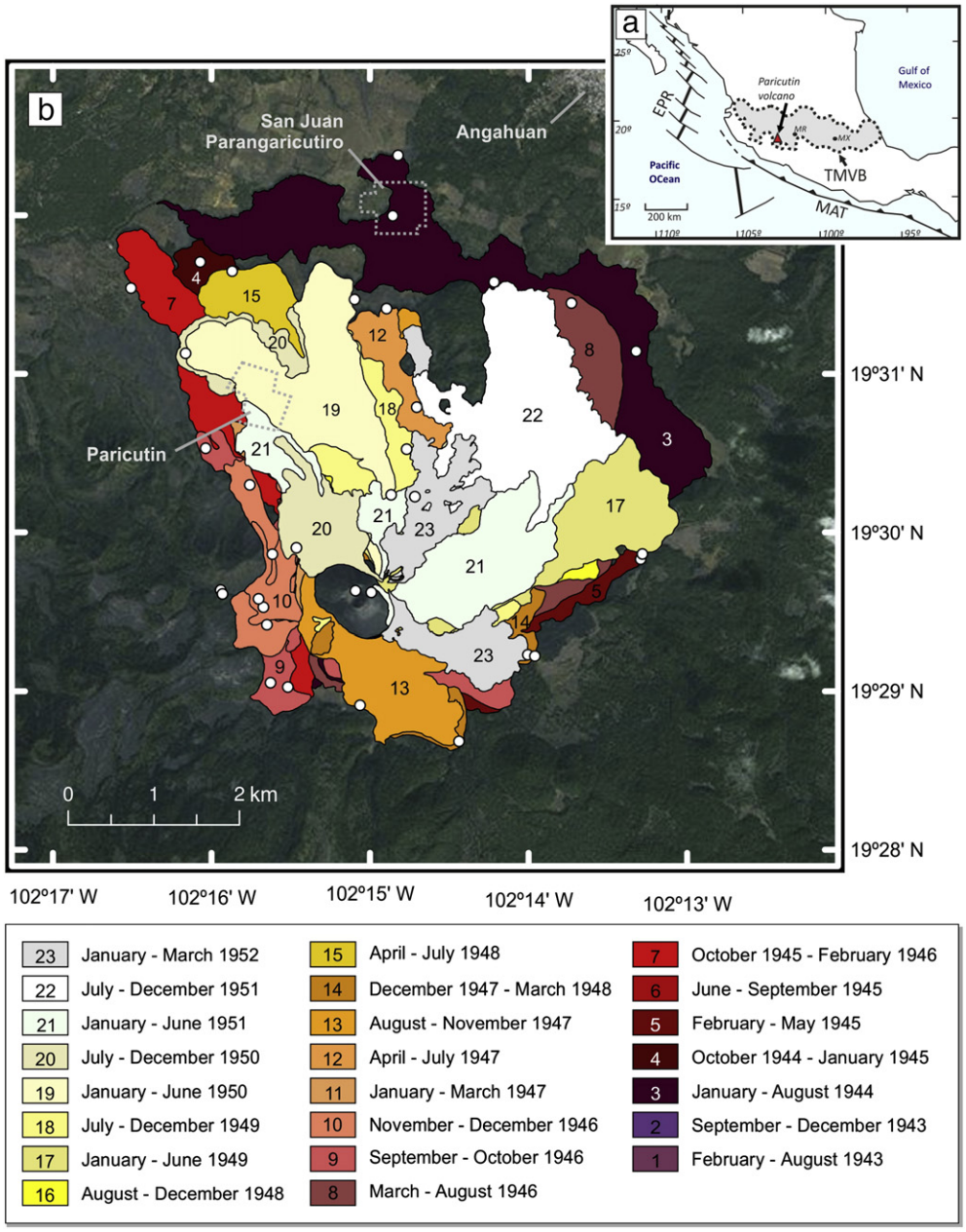

Fig. 1. A) General geotectonic map of Mexico with the location of the Trans-Mexican Volcanic Belt (TMVB), Mexico City (MX), Morelia (MR) and Paricutin volcano. Middle America Trench (MAT), East Pacific Rise (EPR). B) Geological map of the Paricutin volcano representing the 23 eruptive phases modified from Luhr and Simkin (1993), including the sample locations from this study as white circles (see Table 2 for coordinates). Note that lava flows 1, 2, 6, 11, and 16 are no longer exposed on the surface (see Section 3.2. for details). This map was created using ArcGIS® software by Esri. ArcGIS® and ArcMap™.

as Jorullo, Tacámbaro and Zacapu (Guilbaud et al., 2011; Guilbaud et al., 2012; Mahgoub et al., 2017b). Additionally, the spatial and temporal distribution of the different volcanoes, together with the study of their eruptive style and the magmatic processes involved in their formation are critical to better understand the formation and evolution of the MGVF.

This paper focuses on Paricutin volcano, the youngest scoria cone of the MGVF, located ~320 km west of Mexico City at latitude 19°29′35″N and longitude 102°15′05″W (Fig. 1a). Its eruption started in a cornfield on the 20th of February 1943 and ended 9 years later on the 4th of March 1952 (Luhr and Simkin, 1993). The formation and evolution of this volcano captured the interest of scientists world-wide, making Paricutin one of the most outstanding examples for understanding the origin, eruption dynamics, and evolution of monogenetic scoria cones. Shortly after the beginning of the eruption, geologists from several institutions including the U.S. Geological Survey and the Universidad Nacional Autónoma de México surveyed in detail all of the eruptive phases in progress. They monitored the growth of the cone, mapped the lava flows, and took samples and photographs during the nine years of eruptive activity. After the first descriptive works published while the volcano was still active or shortly after the cessation of its activity (e.g. Segerstrom, 1950; Williams, 1950; Wilcox, 1950; Fries, 1953; Foshag and González-Reyna, 1956), more than thirty years passed before more detailed studies focusing on petrology and geochemistry (e.g. McBirney et al., 1987; Bannister et al., 1998; Luhr, 2001; Erlund et al., 2010; Cebriá et al., 2011; Rowe et al., 2011) and the physical

and geomorphological evolution of the volcano (Scandone, 1979; Inbar et al., 1994; Pioli et al., 2008; Dóniz-Páez et al., 2013) were undertaken.

In this work, we focus on the development of Paricutin's complex lava flow field. For this purpose, we have synthesized all of the previous material available and present a compilation of the lava flow maps published by Luhr and Simkin (1993), treating them with a new methodological approach. Geographic Information System (GIS) tools have been combined with modern mapping techniques to facilitate the identification and sampling of all exposed Paricutin effusive eruptive phases as originally defined by Luhr and Simkin (1993). In addition, we present a volumetric study of the lava field including each of the 23 defined eruptive phases, and link them to the geochemical composition of the different lava flows (Larrea et al., in preparation), and other parameters including effusion rate and effective viscosity. Together, these studies provide the first comprehensive documentation of the temporal-volumetric-chemical evolution of the Paricutin lava flow field. Our refined results will allow comparisons with scoria cones in other areas within the MGVF and the TMVB, as well as in other volcanic arcs globally, in order to provide a better understanding of the main factors controlling the formation and evolution of monogenetic fields.

2. The Paricutin eruption and its lava field development

The first sign of volcanic unrest started two weeks before the outbreak of the eruption on the 20th of February 1943 (Foshag and González-Reyna, 1956) in the form of local seismicity that increased in intensity before ending abruptly with the first ejection of magma. The vent opened as a fracture in a flat area, allowing rapid growth of the cone at first; after six days the cone reached a height of 167 m and measured 730 m across its base (Luhr and Simkin, 1993). Subsequently, the rate of pyroclast ejection decreased and lava began to erupt with a variable discharge rate, associated with an overall progressive reduction of the eruption rate and a decrease in the relative proportions of erupted tephra to lava mass (Pioli et al., 2008). By the end of the eruption on the 4th of March 1952, previous estimates suggest that a total area of 233 km^2 (included within the 25-centimeter ash fallout isopach; Segerstrom, 1950) was covered by ~1.38 km^3 of volcanic rock, including lavas and tephra (McBirney et al., 1987), based on the weight calculation by Fries (1953) and considering a magma with a density of 2.6 g/cm^3. Two towns, Paricutin and San Juan Parangaricutiro (Fig. 1b), were buried by lava leading to the evacuation and permanent relocation of their inhabitants in the two new towns of Caltzontzin and San Juan Nuevo.

Throughout the entire duration of the eruption, a cast of scientists (e.g. Adán Pérez-Peña, Jenaro González-Reyna, Ezequiel Ordóñez, William Foshag, Konrad Krauskopf, Kenneth Segerstrom, Howel Williams, Ray Wilcox, etc.) surveyed the progression of the eruption and provided maps depicting the volcano's sequential growth. They collected in-situ samples of the emitted lavas and tephra, took photographs, and partially filmed the eruption during the nine years of eruptive activity. Currently, a large set of the collected samples is stored at the Department of Mineral Sciences of the Natural History Museum of the Smithsonian Institution, located in Washington DC (USA). Later, this information together with testimonies by eyewitnesses were compiled by James Luhr and Tom Simkin in a review book (Luhr and Simkin, 1993) that is currently considered the best documentation of the formation and evolution of the Paricutin volcano.

Luhr and Simkin (1993) divided the development of the lava field into 23 eruptive phases by date of eruption (Figs. 1, 2, and 3). Each eruptive phase is defined by a map sketched by hand at the time of the eruption that delimits the area covered by the lava flow(s) formed during that period, and the total extension of the lava field to date. Most maps contain a unique coordinate point (e.g. 19° 32′ 43.9″ N, 102° 15′ 22.5″ W) and an intersection grid with two km spacing, which were crucial for the georeferencing process in GIS (see Section 3.1 below). From these original maps (see Luhr and Simkin, 1993), we obtained a unique sequence of illustrations that show in detail the lava field development during the entire life cycle of Paricutin.

3. Methods and data sets

3.1. GIS work: the new map and lava volume estimates

Lava fields are formed by the superposition and partial overlapping of numerous individual flow units issued periodically or continuously throughout the duration of an eruption. In many cases, it is difficult to generate maps of individual flows or eruptive phases, as the outlines of earlier lava flows are often obscured by later flows and/or variable degrees of erosive remodeling (Fig. 3). In the case of Paricutin, the detailed information compiled by Luhr and Simkin (1993) for the entire duration of the eruption made this task achievable. Our goal was to create a geological map of the Paricutin eruption, via the digitization and georeferencing of the maps representing the 23 defined eruptive phases (Luhr and Simkin, 1993), using the unique coordinate found on each map as the first control point. New control points were added every 2 km to the East and South to form a grid of control points. In addition, extra control points were created based on geomorphological features clearly observable on both the base-map and the high-resolution scanned maps. The next step involved the creation of a geodatabase (Geographic Coordinate system WGS 1984) and the digitization of the polygons representing each lava flow. This process was repeated with all of the maps representing the 23 eruptive phases, thus obtaining the first volcano-stratigraphic map of the Paricutin eruption (Fig. 1b). The Fisher and Schmincke (1984) nomenclature for types of volcanic activity is used throughout the text for consistency.

In order to estimate the emitted volumes during each eruptive phase, the pre-eruptive topography was reconstructed for every single phase. Three topographic maps were available as starting documents: (1) INEGI (*Instituto Nacional de Estadística, Geografía e Informática)* E13B29 1:50,000 topographic map (2015 edition; contour intervals: 20 m; WGS_1984 UTM); (2) 1:10,000 USGS topographic map (USGS Bull. Vol. 965; 1956; contour intervals: 5 m) made from the aerial photographs taken by *Compañía Mexicana Aerofoto S.A.* in 1934 for the agricultural credit bank; (3) 1:10,000 USGS topographic map (USGS Bull. Vol. 965; 1956; contours interval: 5 m) made from the aerial photographs taken by *Compañía Mexicana Aerofoto S.A.* in 1946 for the US Geological Survey.

Map (2) represents the pre-Paricutin topography in 1943, and map (3) the topography in 1946 (intermediate topographic survey during the course of the eruption). Both maps were georeferenced using the current topography represented by map (1), i.e., simple physical features were used to project them on the UTM WGS 1984 coordinate system. This solution was the most appropriate due to the current existence of a thick layer of ash, the lack of surface deformation measurements in the area, and the absence of information about the projections used during the elaboration of the UGSG maps. Maps (2) and (3) could not be georeferenced solely by geographic coordinates, due to the high residual error obtained for this georeferencing process (x: 2.2–0.9 and y: 4.5–0.4; root mean square error: 2.5–0.7).

The different lava flow units within each eruptive phase as defined by Luhr and Simkin (1993) were subsequently redrawn (delimited) considering previously unavailable morphological details of the lava flows (e.g. flow fronts, leeves, compression ridges, etc.). The palaeogeomorphological reconstruction of the lava flows from the eruptive phases 15 to 23 were also revised based on the new currently available topographic maps together with the high resolution 2015 Google Earth satellite imagery (Fig. 2b). Lava flows from the intermediate eruptive phases 4 to 15 were reconstructed with the information provided by the map (3) (USGS 1946; USGS Bull., Vol. 965, 1956) (Fig. 2a). The oldest lava flows from eruptive phases 1 to 3 were carefully modelled using the information provided by map (2) (Fig. 2a).

By using the pre-eruption topography and knowing the accurate areal distribution (limit) of each eruptive phase, it was possible to restore the ideal paleotopography of each lava flow unit. This paleotopographic reconstruction process complied with the following rules:

- The tool "*clip*" was used to remove the contour lines within the polygon representing each lava flow.
- The contour lines inside each polygon were "reconstructed" taking into account the principle of continuity to the nearest contour line, the average thickness reported for each lava flow (Table 1; Luhr and Simkin, 1993), the shape of the contour lines of other lava flows (i.e., we tried to simulate the sinuosity of the contour lines of flows not covered by younger products), and in all cases, it was essential not to exceed the maximum height and length of each lava flow according to the historic records by Luhr and Simkin (1993).

Once we had obtained the topography "without lava flows" and "with lava flows" for each eruptive phase, the digital elevation models (DEMs) (Fig. 2) were calculated as a triangular irregular network (TIN) map. Subsequently, the tool "*surface difference*" was used to calculate the volumetric difference (positive and negative) between two consecutive DEMs. The errors associated with regular interpolation processes can be up to 10 m in thickness ("z") when calculating digital elevation models (Pérez-Vega and François-Mas, 2009); however, the TIN model minimizes the maximum internal angle, providing a more equitable triangulation for each data point (Tucker et al., 2001). For this reason, the calculated values are considered the most precise minimum values to date. As a result, the reconstructed topography is more homogenous but still considers slope variations. Therefore, the volumes obtained with the tool "*surface difference*" are calculated utilizing the minimum closest value to the "real values" of the geometrizing method (volume = area × average thickness; see Guilbaud et al., 2012). Additional minor intrinsic errors in the reconstructions based on in-situ observations are difficult to quantify, thus the calculations should be considered semi-quantitative. The estimated volumes erupted in each eruptive phase are reported in Table 1. Utilizing this new information, we have also calculated magma effusion rates with more precise temporal and spatial scales (note that the effusion rate calculation in most cases includes several lava flows; see Section 3.3).

3.2. Fieldwork and sampling strategy

During the March and November 2015 fieldwork campaigns the GIS-based Paricutin volcano-stratigraphic map was used to facilitate the identification of the 23 different eruptive phases in the field, and the sampling of the missing eruptive phases from the preliminary 2012 fieldwork campaign (Fig. 3). The GIS map was uploaded to the Miami University ArcGIS online cloud and shared with the Collector for ArcGIS App. This App, which can be installed on any smartphone or tablet device, allows the interaction with the map when offline during fieldwork. The App uses the GPS signal of the mobile device to indicate the user's real-time location on the map, confirming one's exact position on the eruptive deposits of any given eruptive phase required for sampling.

Using this methodology, we had precise information about the eruptive phases that were no longer exposed on the surface (i.e., eruptive phases: 1, 2, 6, 11, and 16; Fig.1). Accordingly, samples from these covered eruptive phases were requested from the Smithsonian Museum of Natural History, in order to have at least one sample from each eruptive phase that defined the time span of Paricutin's activity (Table 2). Unfortunately, samples from eruptive phases 2 and 11 were not available at the Smithsonian Museum.

3.3. Chemical and petrophysical analysis

A total of 31 lava flows from 21 of the 23 eruptive phases were analyzed for whole rock major element compositions (see Table 2). Samples were first cut into thin slabs, ground with silicon carbide sand paper to remove any metal traces from the rock saw, and cleaned thoroughly with 18 MΩ H_2O in an ultrasonic bath. The samples were dried in an oven at 110 °C, then crushed in an alumina jaw-crusher and powdered in a high-purity alumina shatter box at Miami University (Ohio, USA). Major elements were analyzed by X-ray fluorescence spectrometry (XRF) at the GeoAnalytical Laboratory at Washington State University. Details of the sample preparation, analytical procedures, detection limits, precision and accuracy, and geochemical reference standards are provided on the Peter Hooper GeoAnalytical Lab website (http://cahnrs.wsu.edu/soe/facilities/geoanalytical-lab/). The mean composition of each eruptive phase was calculated taking into account the major element compositions of all the lava flow samples collected from the same eruptive phase (see Table 2). The complete chemical dataset, which includes all trace elements and Sr-Nd-Pb-Os isotopic data, will be discussed in a forthcoming paper focused on the petrogenesis of Paricutin volcano (Larrea et al., in preparation).

The morphological features, chemical composition, crystal cargo and modal percentage, and vesicle size of each lava flow are relevant parameters used to calculate petrophysical values such as effusion rate and viscosity (Pyle and Elliot, 2006). Thin sections were prepared to estimate modal percentages and the size of phenocrysts (>2 mm) and microphenocrysts (0.2–2 mm) for each lava flow. The effective viscosity of the magma was calculated using Ken Wohletz's "Magma" program (http://www.lanl.gov/orgs/ees/geodynamics/Wohletz/KWare/Index.htm) based on the Bottinga and Weill (1972) model (Table 2). Input parameters (Table 2) for this calculation include modal percentage of crystals, chemical composition and water content of the magma (~2.2 wt% H_2O based on phase-equilibrium experiments by Eggler, 1972, in accordance with water in melt inclusions as determined by Luhr, 2001 and Pioli et al., 2008. These effective viscosity calculations do not account for vesicle content, vesicle distribution or vesicle shapes. The effusion rate (m^3/s) is an important parameter to understand magma system dynamics (Dvorak and Dzurisin, 1993; Harris et al., 2007) and a useful tool to predict the velocity and forecast the behavior of future effusive eruptions, and therefore predict related hazards and design mitigation plans (Rowland et al., 2003; Rodriguez-Gonzalez et al., 2010).

4. Results

4.1. Volumes of the Paricutin volcano lava field

The Paricutin lava field has a shield-like topographic profile that is 5 km across and rises up to 245 m above the 1943 topographic surface. At any given time during the eruption, usually only one or a few flows or flow lobes were active, advancing slowly and extending in the general direction of the pre-eruption regional slope. Lava flows extended farthest from the main cone towards the north and east, however, the majority of the flows were emitted from fissure vents at the SW and NE foot of the main cone.

With the aid of the new GIS-based map we calculated the total lava volume emitted during the 9 years of eruption, and the volume of lava

Fig. 2. Reconstruction of Paricutin's topographic evolution with time, showing the DEM maps of the 23 eruptive phases defined within the Paricutin's lava flow field: A) Eruptive phases 1–11 and B) eruptive phases 12–23. Each eruptive phase is defined by the pre-eruptive phase topography and the new lava flow extension (red polygon), allowing a better understanding of the geomorphologic evolution of the area as the volcanic activity progressed. Note: inferred location of main fissure vents at the SW and NE foot of the cone are plotted in Fig. 2a - pre-eruption topography phase; secondary vents linked to continuation of previous eruptive phase lava flows are omitted for clarity (i.e., little polygons in Fig. 2a - eruptive phase 9, Fig. 2b - eruptive phase 13, 14, 15, 18, 20, 21 and 23). AG: Angahuan; SJP: San Juan Parangaricutiro; P: Paricutin.

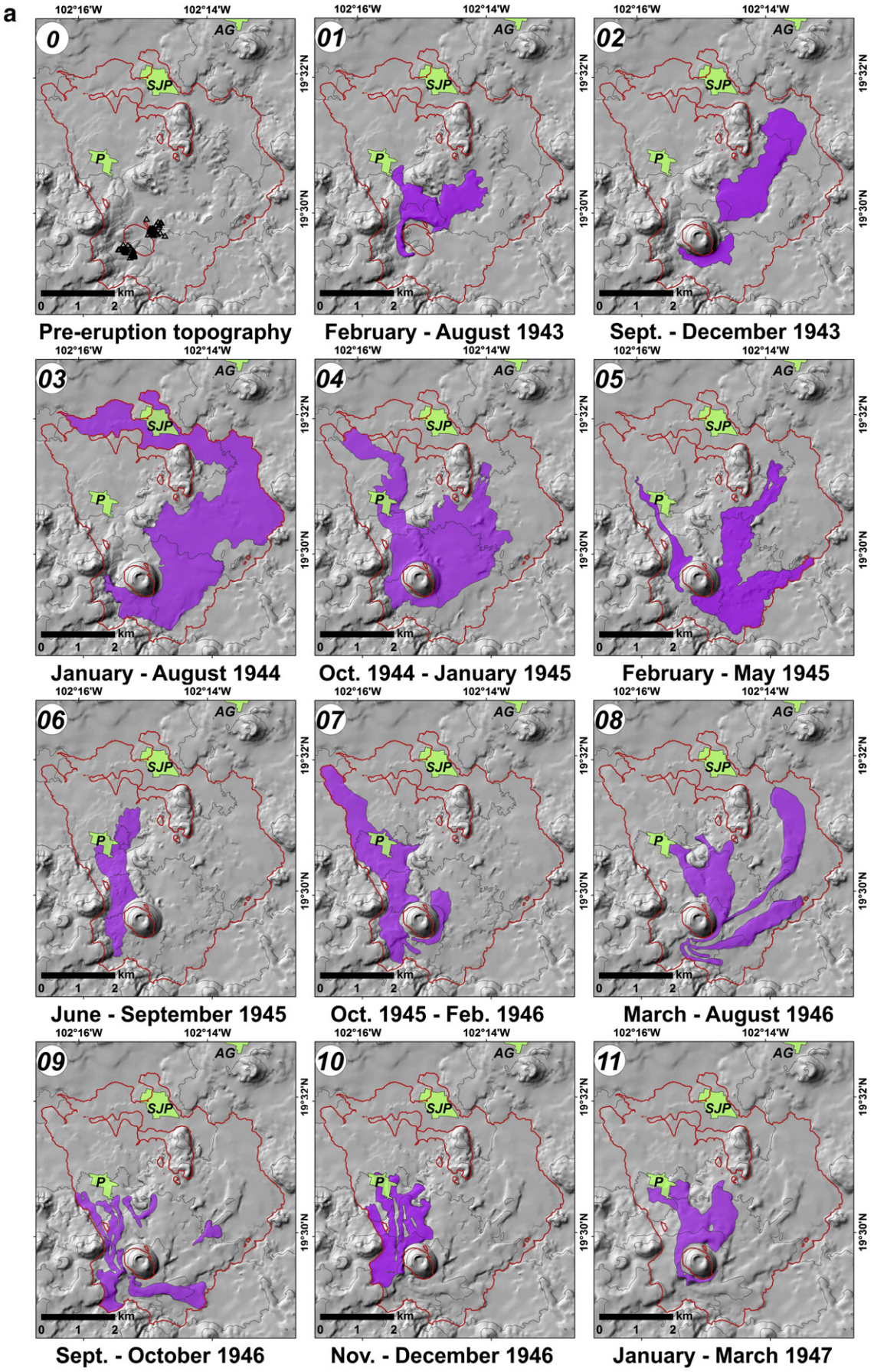
a
0
Pre-eruption topography
01
February - August 1943
02
Sept. - December 1943
03
January - August 1944
04
Oct. 1944 - January 1945
05
February - May 1945
06
June - September 1945
07
Oct. 1945 - Feb. 1946
08
March - August 1946
09
Sept. - October 1946
10
Nov. - December 1946
11
January - March 1947
AG
SJP
P
102°16'W
102°14'W
19°32'N
19°30'N
km
0 1 2

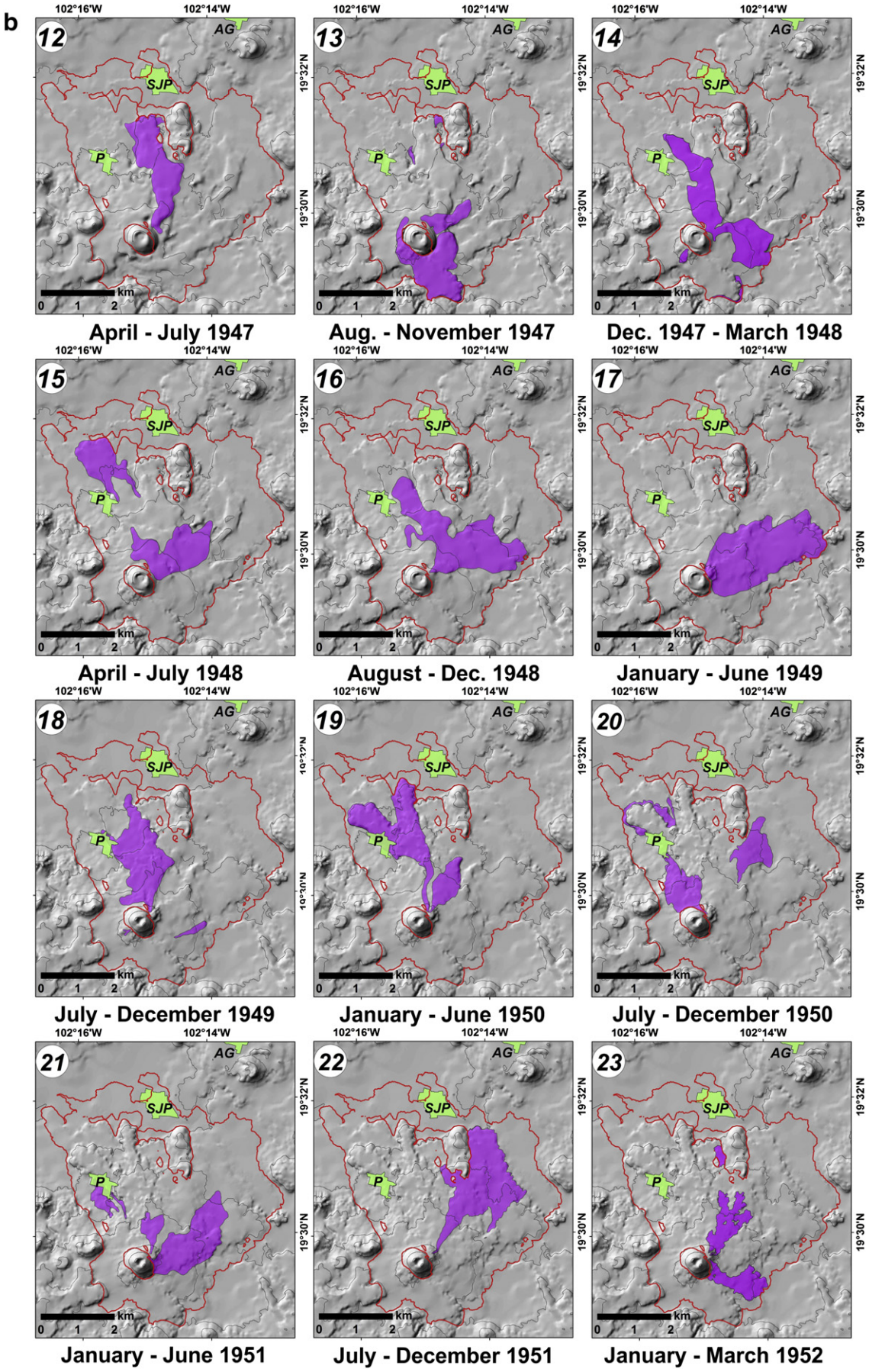

Fig. 2 (*continued*).

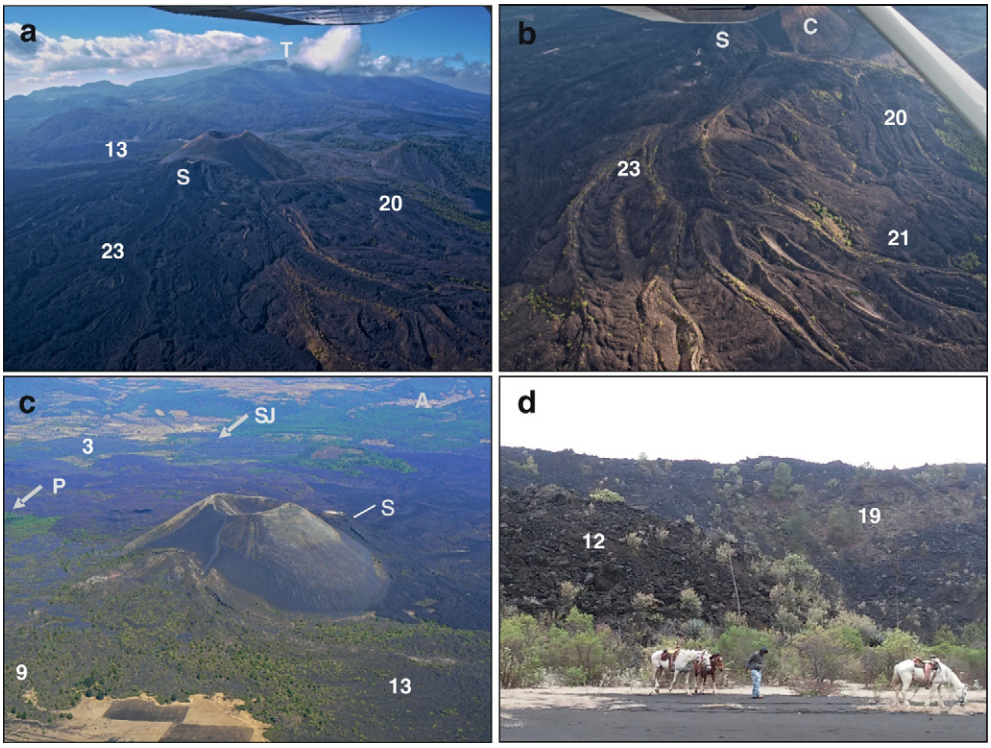

Fig. 3. Features of the Paricutin lava flow field (numbers denote lava flows pertaining to different eruptive phases, as defined in Figs. 1 and 2). a) Aerial view of Paricutin and the proximal sector of its lava flow field from the north. Tancítaro stratovolcano (T) and Sapichu vent (S) are also shown. Photo taken February 01, 2009 by Lorely Galván. b) Aerial photo showing complex details (pressure ridges, levees, etc.) of superimposed lobes of the lava flow field. The Sapichu vent (S) and Paricutin's main cone (C) are indicated. Photo taken January 31, 2009 by Lorely Galván. c) Aerial view of Paricutin from the south. Town of Angahuan (A) and Sapichu vent (S). Yellow arrows denote locations of the buried towns of Paricutin (P) and San Juan Parangaricutiro (SJ). Photo taken February 07, 2010 by Claus Siebe. d) Distal lava flow fronts in the NW sector of the lava field. Photo taken March 16, 2015 at the PAR-1522 sample location by Patricia Larrea.

extruded during each of the 23 eruptive phases defined by Luhr and Simkin (1993) (see Section 3.1 for further details). These estimated volumes are not dense rock equivalent (DRE) volumes, because they include void spaces (i.e., vesicles and fractures). In Table 1 we have reported a summary of the average thickness, areal extent and the DEM-aided volume calculated for each eruptive phase. The estimated erupted volume (colored bars) and the cumulative volume (grey bars) for each eruptive phase vs. time are represented in Fig. 4a.

Table 1
Summary of the reported average thickness, and calculated surface area, volume and average lava eruption rate for each eruptive phase of Paricutin volcano.

Eruptive phase	Dates	Average thickness (m)	Area[a] (m^2)	DEM-aided calculated volume (km^3)
1	February–August 1943	15[c]	2,373,477	0.067
2	September–December 1943	From 5 to 10[b]	3,647,868	0.064
3	January–August 1944	20[c]	12,317,807	0.300
4	October 1944–January 1945	15[b]	8,175,116	0.126
5	February–May 1945	From 10 to 15[c]	5,147,302	0.043
6	June–September 1945	10[c]	2,316,008	0.024
7	October 1945–February 1946	From 20 to 25[c]	4,536,518	0.111
8	March–August 1946	10[b]	5,089,923	0.104
9	September–October 1946	From 10 to 25[c]	2,925,262	0.041
10	November–December 1946	20[b]	3,273,536	0.059
11	January–March 1947	20[c]	2,650,329	0.042
12	April–July 1947	20[b]	2,152,303	0.063
13	August–November 1947	From 10 to 13[b]	2,628,313	0.119
14	December 1947 - Mar, 1948	From 10 to 18[b]	3,072,912	0.063
15	April–July 1948	From 10 to 25[c]	3,292,831	0.050
16	August–December 1948	10[b]	3,811,855	0.045
17	January–June 1949	9[b]	4,479,017	0.123
18	July–December 1949	From 10 to 12[b]	2,718,243	0.039
19	January–June 1950	From 20[b] to 30[c]	3,393,513	0.150
20	July–December 1950	From 8 to 20[b]	2,358,689	0.048
21	January–June 1951	7[b]	2,986,401	0.047
22	July–December 1951	7[b]	3,492,196	0.026
23	January–March 1952	8[b]	1,892,357	0.010
			Total	1.764

Note: The DEM-aided volume was obtained by subtracting the pre-eruption topography from the actual topography (see Methods and data sets).
[a] Obtained from the supplemental topographic map published by the USGS (Bull, Vol, 965, 1956) and Luhr and Simkin (1993).
[b] Thickness estimated by direct observation in the field as reported by Luhr and Simkin (1993).
[c] Thickness estimated by making profiles with the aid of the digital elevation model.

Table 2
Whole rock major element compositions, modal percentage of crystals > 0.2 mm, effective viscosity and effusion rate of the lavas collected from each eruptive phase*. The average (Avg.) compositions represent the mean composition of each eruptive phase considering all the lava flows collected from the same eruptive phase.

Eruptive phase	Avg. SiO_2	Avg. MgO	Sample name	Coordinates	SiO_2	TiO_2	Al_2O_3	$FeO^{(t)}$	MnO	MgO	CaO	Na_2O	K_2O	P_2O_5	TOTAL	Modal percentage of crystals > 0.2 mm	Effective viscosity (Pa·s)	Effusion rate (m^3/s)
1	53.9	7.1	NMNH116291-2	[a]	53.87	0.91	17.96	7.13	0.13	7.06	7.90	3.86	0.77	0.21	99.80	–	–	4.0
3	55.7	5.5	PAR-1206	19° 31.143′ N 102° 13.311′ W	55.53	1.08	17.36	7.40	0.13	5.46	6.86	4.10	1.20	0.35	99.47	8	1090	14.2
			PAR-1214	19° 31.991′ N 102° 14.833′ W	55.87	1.08	17.44	7.39	0.13	5.50	6.90	4.16	1.20	0.35	100.02	8	1090	14.2
			PAR-1215	19° 32.368′ N 102° 14.800′ W	55.66	1.07	17.36	7.34	0.13	5.49	6.88	4.13	1.20	0.35	99.61	8	1080	14.2
4	55.9	5.7	PAR-1530	19° 31′ 40,1″ N 102° 15′ 56,0″ W	55.90	1.05	17.30	7.30	0.13	5.67	6.91	4.10	1.22	0.34	99.92	3	930	11.9
5	56.4	5.6	PAR-1203	19° 29.242′ N 102° 13.946′ W	56.41	1.01	17.37	6.88	0.12	5.57	6.98	4.03	1.26	0.33	99.96	5	900	4.2
			PAR-1204	19° 29.838′ N 102° 13.290′ W	56.46	1.01	17.34	6.92	0.12	5.53	6.98	4.03	1.26	0.33	99.98	5	910	4.2
6	56.2	5.7	NMNH 116295-3	[a]	56.23	0.97	17.14	6.81	0.12	5.73	6.93	4.02	1.24	0.3	99.49	–	–	2.2
7	56.8	5.5	PAR-1216	19° 31.539′ N 102° 16.470′ W	56.78	0.93	17.23	6.52	0.12	5.48	6.81	4.00	1.25	0.30	99.42	–	–	8.5
8	57.4	5.4	PAR-1517	19° 31′ 20,7″ N 102° 13′ 42,7″ W	57.43	0.88	17.19	6.24	0.12	5.43	6.70	4.04	1.26	0.28	99.57	3	1180	6.5
9	57.5	5.3	PAR-1526	19° 29′ 03,9″ N 102° 15′ 29,1″ W	57.50	0.86	17.18	6.44	0.11	5.27	6.68	3.95	1.27	0.27	99.53	5	1310	7.8
			PAR-1528	19° 30′ 35,8″ N 102° 16′ 03,1″ W	57.46	0.86	17.21	6.38	0.11	5.39	6.72	3.95	1.27	0.27	99.62	5	1270	7.8
10	57.1	5.5	PAR-1210	19° 29.431′ N 102° 15.619′ W	57.19	0.87	17.17	6.44	0.11	5.41	6.69	3.95	1.27	0.28	99.38	7	1320	11.2
			PAR-1213	19° 30.307′ N 102° 15.727′ W	57.09	0.87	17.14	6.42	0.11	5.35	6.71	3.96	1.27	0.28	99.20	7	1310	11.2
			PAR-1211	19° 29.542′ N 102° 15.643′ W	57.09	0.87	17.16	6.52	0.11	5.58	6.72	3.92	1.27	0.27	99.51	7	1260	11.2
			PAR-1212	19° 29.593′ N 102° 15.672′ W	56.97	0.87	17.12	6.47	0.11	5.53	6.69	3.94	1.27	0.27	99.24	7	1270	11.2
12	57.8	5.0	PAR-1518	19° 30′ 48,5″ N 102° 14′ 41,1″ W	57.84	0.86	17.51	6.24	0.11	4.83	6.79	3.96	1.29	0.27	99.70	5	1430	6.0
			PAR-1522	19° 31′ 24,4″ N 102° 14′ 56,3″ W	57.69	0.87	17.44	6.25	0.11	5.10	6.79	3.96	1.28	0.27	99.76	5	1350	6.0
13	58.2	4.1	PAR-1525	19° 28′ 57,1″ N 102° 15′ 09,1″ W	58.24	0.85	17.71	6.35	0.11	4.13	6.69	4.03	1.34	0.27	99.72	2	1610	11.3
14	58.3	4.1	PAR-1201	19° 28.705′ N 102° 14.420′ W	57.91	0.85	17.64	6.39	0.11	4.25	6.65	4.08	1.34	0.28	99.50	3	1460	6.0
			PAR-1202	19° 29.251′ N 102° 13.988′ W	58.71	0.84	17.50	6.15	0.11	4.03	6.45	4.06	1.42	0.29	99.56	3	1840	6.0
15	58.9	4.1	PAR-1529	19° 31′ 40,3″ N 102° 15′ 54,0″ W	58.85	0.83	17.24	6.16	0.11	4.05	6.40	4.09	1.46	0.29	99.48	3	1830	4.7
16	59.2	4.0	NMNH 116295-34	[a]	59.17	0.83	17.37	6.10	0.11	4.02	6.43	4.05	1.47	0.29	99.84	–	–	3.4
17	58.9	3.8	PAR-1205	19° 29.880′ N 102° 13.275′ W	58.92	0.83	17.23	6.07	0.11	3.78	6.30	4.01	1.50	0.30	99.05	3	2030	7.9
18	60.0	3.6	PAR-1521	19° 30′ 30,9″ N 102° 14′ 46,5″ W	60.00	0.81	17.30	5.82	0.11	3.57	6.24	4.08	1.58	0.28	99.79	2	2230	2.5
19	59.6	3.7	PAR-1523	19° 31′ 27,7″ N 102° 15′ 06,3″ W	59.62	0.81	17.18	5.80	0.11	3.71	6.27	4.19	1.56	0.28	99.53	2	2040	9.6
20	60.0	3.6	PAR-1524	19° 31′ 08,7″ N 102° 16′ 12,5″ W	59.83	0.81	17.23	5.99	0.11	3.59	6.23	4.01	1.58	0.28	99.66	2	2220	3.0
			PAR-1527	19° 29′ 54,8″ N 102° 15′ 26,4″ W	60.18	0.81	17.22	5.69	0.10	3.54	6.18	4.03	1.60	0.27	99.62	2	2330	3.0
21	60.1	3.5	PAR-1519	19° 30′ 15,5″ N 102° 14′ 49,5″ W	60.08	0.80	17.23	5.63	0.10	3.54	6.15	3.96	1.60	0.27	99.36	2	2380	3.6
22	60.5	3.5	PAR-1207	19° 31.575′ N 102° 14.200′ W	60.48	0.81	17.32	5.85	0.10	3.53	6.13	4.04	1.63	0.28	100.17	–	–	1.6
23	59.9	3.7	PAR-1520	19° 30′ 14,6″ N 102° 14′ 45,9″ W	59.93	0.80	17.13	5.60	0.10	3.70	6.11	3.98	1.61	0.26	99.22	–	–	1.5

Note that there are not samples from eruptive phases 2 and 11, as these eruptive phases are no longer exposed in the field, and the Smithsonian did not have samples available from these periods of time.
Effective viscosity was calculated according to Ken Wohletz's "Magma" program (http://www.lanl.gov/orgs/ees/geodynamics/Wohletz/KWare/Index.htm) based on Bottinga and Weill (1972) model.
[a] Samples provided by the Department of Mineral Sciences of the Smithsonian Institution.

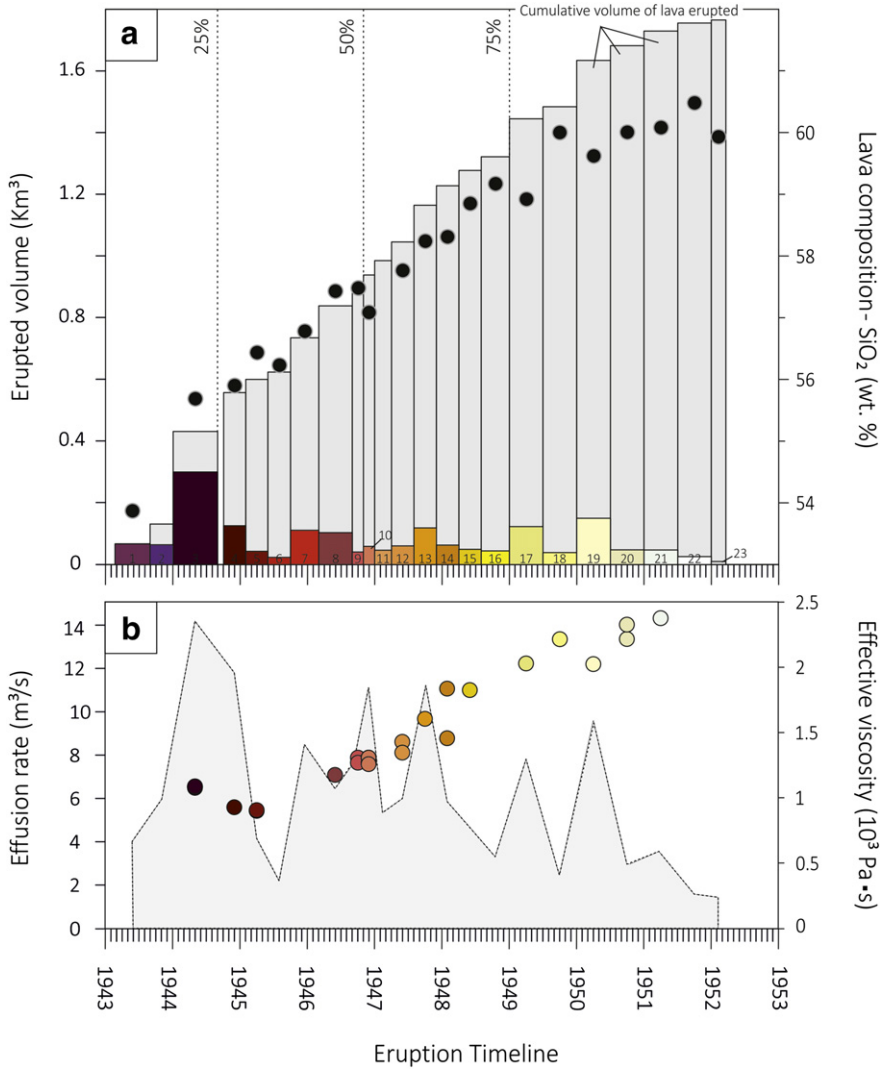

Fig. 4. A) Graph showing the eruption timeline, volume erupted, and average chemical composition (black dots) of the 23 eruptive phases defined by Luhr and Simkin (1993). Note that grey bars represent the cumulative volume of lava erupted with time, marking when the 25%, 50% and 75% of the total volume emitted by Paricutin was erupted for reference. B) Graph showing effusion rate (m^3/s) and effective viscosity (10^3 Pa·s) (dotted line) for each eruptive phase (Table 2). Note that some effective viscosity values are not shown due to the absence of geochemical and/or petrological data.

The Paricutin lava field covers 25 km^2 with an estimated total volume of 1.764 km^3, and an average daily volume of erupted lava that ranged from $1.2 \cdot 10^{-3}$ km^3 to $1.26 \cdot 10^{-4}$ km^3. As observed in Fig. 4a, the extruded volumes of lava were highly variable with time; only seven eruptive phases emitted >0.1 km^3 of lava (i.e. eruptive phases 3, 4, 7, 8, 13, 17, and 19, see Fig. 2), over variable periods of time ranging from 122 to 244 days (Table 1; Fig. 4a). The largest volume emitted by Paricutin in a single eruptive phase took place from January to August 1944 (eruptive phase 3, see Fig. 2a) causing the burial of the town of San Juan Parangaricutiro, whereas most of the small volume eruptive phases occurred after the second half of 1950. In <2 years, more than the 25% of the total volume of lava was emitted, and by November 1946 (three years and 10 months after the beginning of the eruption) more than the 50% of the total volume had been erupted. Accordingly, the remaining 50% of the volume was extruded during the last 5 years of the eruption. Fries (1953) proposed that the effusion rate decreased progressively with time, however, our new data (Table 2; Fig. 4b - grey polygon) shows fluctuation between 2 and 14 m^3/s, with the only real decrease after 1950. In accordance with the highest volumes, the highest effusion rate (14.2 m^3/s) also corresponds to eruptive phase 3 (Figs. 2a and 4a–b). In contrast, the lowest effusion rates were 1.6 and 1.5 m^3/s, occurring during the last two eruptive phases (22 and 23) (Figs. 2b and 4b).

4.2. Chemical composition of the volcano

The GIS-based Paricutin volcano stratigraphic map together with the Collector for ArcGIS App facilitated the identification and sampling of eighteen eruptive phases during our fieldwork campaigns. Moreover, samples from three eruptive phases no longer exposed in the field were obtained from the Smithsonian Museum of Natural History. Although two eruptive phases are missing in this study (2 and 11), this work comprises the most comprehensive collection of lavas from Paricutin volcano to date, allowing for a detailed reconstruction of the temporal, areal, and chemical development of the lava field (Fig. 2; Table 2).

Paricutin lavas range in composition from basaltic-andesite to andesite following the TAS classification by Le Bas et al. (1986) (Fig. 5), and belong to the medium-K series, in agreement with previously published data (e.g. McBirney et al., 1987; Cebriá et al., 2011; Rowe et al., 2011). All lavas erupted during the first three years of the eruption (phases 1 to 10) are basaltic andesites, but after 1946 only andesites

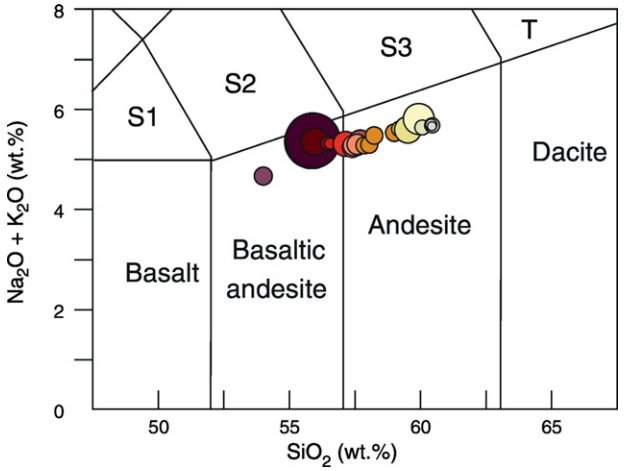

Fig. 5. Total alkalis vs. SiO_2 (TAS) diagram for Paricutin lava flows (after Le Bas et al., 1986). Legend as in Fig. 1; note symbol size proportional to the calculated volume of each eruptive phase.

were erupted. Taking into account the emitted volumes, basaltic andesite is the most abundant lava composition (53.2 vol% - 0.939 km^3) emitted by Paricutin, comprising 46.8 vol% (0.825 km^3) of the total volume (lava and tephra).

Accordingly, the eruptive products also show a progressive change in mineralogy, starting as olivine-bearing basaltic andesites and evolving to orthopyroxene and clinopyroxene-bearing andesites containing <1% olivine by the end of the eruption. The modal percentages of phenocrysts and microphenocrysts range from 2 to 8 vol%. The last eruptive phases (eruptive phases 18–23) present the lowest proportions of crystals (<2%), whereas the early lavas (eruptive phase 3) present the highest crystal cargo (~8%). These data, together with the geochemistry of each eruptive phase and magma water content (2.2 wt%), were used to calculate the effective viscosity of the lava flow (Table 2), which ranges from 0.9 to $1.84 \cdot 10^3$ Pa·s in the early and intermediate eruptive phases (Fig. 4b). The latest eruptive phases show an increase in effective viscosity with values ranging from 2.03 to $2.38 \cdot 10^3$ Pa·s (Fig. 4b), consistent with increasing silica and crystal contents.

5. Discussion

5.1. Volumetric estimates of the Paricutin eruption

The first estimate of the mass of solids erupted by Paricutin volcano was done by Foshag (1950). His estimate was based only on approximations of cone dimensions and lava volumes for a subset of the eruptive phases, rather than the entire lava field. The first serious attempt to quantify the eruptive volumes of Paricutin was made by Fries (1953), who estimated a total of 3560 metric tons of solids erupted, including 2230 million metric tons of pyroclastic material and about 1330 million metric tons of lava. He also provided the total volume of most lava flows (not including the last flow in 1952) based on the individual lava flow areas and their estimated average thicknesses from personal observations or published descriptions. The estimated total lava flow volume determined by Fries (1953) was 0.7 km^3, although he noted that his estimate was probably too low and subject to errors in mapping and lava flow thickness estimates, pending corrections from topographic maps. Later, Scandone (1979) and McBirney et al. (1987) used the masses reported by Fries (1953) to recalculate the dense rock equivalent (DRE) volume of lavas and tephra assuming a uniform density of 2.7 and 2.6 g/cm^3, respectively. The total volume of magma was estimated at 1.316 km^3 by Scandone (1979) and 1.38 km^3 by McBirney et al. (1987). In both cases an exponential/gradual decrease in annual effusion rate with time was recognized, and interpreted by Scandone (1979) as evidence for a lack of replenishment of the magma chamber following initiation of the eruption in 1943.

Our calculation of 1.764 km^3 of erupted lava, based on the pre-, *syn*-, and post-eruption topographic maps, is likely more reliable than previous estimates. If the volume of the entire lava flow field is converted to dense rock equivalent (DRE) assuming the 5–10 vol% of vesicles determined for the lavas, the minimum volume of erupted Paricutin magma ranges between 1.59 and 1.68 km^3 DRE.

Moreover, the daily volume of erupted material according to Fries (1953) varied from $3.4 \cdot 10^{-4}$ to $9 \cdot 10^{-5}$ km^3, which is also much lower than our calculation of $1.2 \cdot 10^{-3}$ km^3 to $1.26 \cdot 10^{-4}$ km^3 of lava erupted per day. Our calculation should be much more precise because it utilized effusion rates determined for each eruptive phase. Therefore, the Fries (1953) volumetric estimates for the cone (0.25 km^3) and ash blanket (0.64 km^3) might also be in error, as observed for the lava field, when the topographic correction is made.

5.2. Eruptive style and history of Paricutin

The eruption of Paricutin started on the 20th of February 1943 after several weeks of precursory seismicity (Yokoyama and De la Cruz-Reyna, 1990; McBirney et al., 1987). The first vent opened as a fissure crossing a flat area from which continuous low-magnitude pyroclastic activity rapidly produced a cinder cone during the first weeks (Foshag and González-Reyna, 1956). The emission of the first lava flow (Quitzocho flow) started immediately after initiation of the volcanic activity, and thereafter the discharge of lava varied in rate and shifted from one part of the fissure to another. A period of intense explosive activity took place from mid-March to early June 1943, generating large eruptive columns (2–6 km; Pioli et al., 2008) with fine ash deposition reaching as far as Mexico City (Fries, 1953). After June, explosions became more sporadic, but strong explosive activity resumed in late July and continued until mid-October. This time frame (from the 20th of February to the 18th of October 1943 including eruptive phases 1 to 3) is known as the Quitzocho phase, which mostly comprised the construction of the main cone. The Sapichu phase (from the 18th of October 1943 until the 8th of January 1944, eruptive phases 2–3) started with the opening of a new effusive vent (the Sapichu parasitic vent) to the northeast of the main cone, at which time the activity at the main cone ceased. During this time frame, abundant and continuous lava flows were emitted carrying an assortment of crustal xenoliths (Foshag and González-Reyna, 1956; McBirney et al., 1987). After cessation of activity at Sapichu, the Taquí phase started (from the 8th of January 1944 to the 12th of January 1945, eruptive phases 3–4) with the formation of the Taquí and Ahuan vents to the south and east of the main cone, respectively. During this time frame, extended violent Strombolian eruptions occurred and the activity at the main vent resumed but with decreasing frequency. Fries (1953) estimated that almost 80% of the total pyroclastic material (tephra + cone) was already erupted by 1945, as documented by the comparison of the isopach maps produced in May 1945 (Krauskopf and Williams, 1946) and in late 1946 (Segerstrom, 1950). Lastly, from January 1945 to March 1952 (eruptive phases 4–23) activity consisted mostly of irregular, short-lived lava flows, interrupted by Vulcanian explosions after 1949. On the 25th of February 1952, both lava emission and pyroclastic activity ceased abruptly bringing the nine-year eruption of Paricutin volcano to its end.

The style of volcanic eruptive phases in small-volume monogenetic volcanoes is strongly dependent on the influence of internal magmatic parameters (e.g., magmatic volatile content, chemical composition and, effective and relative viscosity) and environmental factors (e.g., presence and relative proportion of external water, host sediment physical conditions and basement fractures) (e.g., Smith and Németh, 2017 and references therein). Notable characteristics of the Paricutin eruption include an erratic variation in effusion rate with an overall increase in the effective viscosity of the magma, and a variation in the importance of effusive

relative to explosive activity throughout the nine years of eruption, accompanied by a progressive change in the bulk magma composition, evolving from an olivine-bearing basaltic andesite with a SiO_2 content of ~54 wt% to a pyroxene-bearing andesite with slightly >60 wt% SiO_2 (Fig. 4). This is a somewhat unexpected behavior, as we would expect an increase in explosivity as more evolved and more viscous magmas are generated. In contrast, in Paricutin the most mafic compositions (first volcanic products) are the ones related to the most explosive activity. Therefore, it is not only the composition and the effective viscosity of the generated magmas that controlled the explosivity of the volcano. The magma pre-eruptive volatile content and the degassing mechanism might be key factors controlling the explosive activity at Paricutin volcano (e.g., Parfitt and Wilson, 1995). Degassing conditions depend on both magma ascent rates and the relative permeabilities of magma and wall rock (Cashman, 2004). In this case, the change from initial explosive activity to effusive activity as the eruption progressed probably took place when slow magma ascent rates accompanied by extensive crystallization allowed near-complete degassing of magma (e.g., Cashman, 2004; Cervantes and Wallace, 2003). This is consistent with observations of Krauskopf (1948), who noted that during eruption of Paricutin lavas, gas escaped through bubbly magma emissions restricted to the central vent of the cone, suggesting that separation of gas from magma occurred at shallow depths within the cone; in constrast, lava emitted from fissure vents near the base of the cone was degassed (Fig. 2a). A similar mechanism was proposed by Cervantes and Wallace (2003) for degassing at Xitle volcano (Mexico) and by Genareau et al. (2010) at Lathrop Wells volcano (USA).

Effusion rates for eruptions of monogenetic volcanoes are, in general, poorly constrained. The overall effusion rate for Paricutin decreases progressively with time (Fig. 4b), although our more precise calculation for each eruptive phase shows fluctuation between 2 and 14 m^3/s, with the only real decrease after 1950. This is significant, because discharge rates are frequently used to infer the duration of similar but older eruptions based on volume estimates (e.g., Lorenzo-Merino et al., in revision). Furthermore, Fig. 4b reveals a lack of direct relationship between discharge rates and magma composition and effective viscosity throughout the eruption. The existence of continuous lava flows in Paricutin could be explained by the overall high eruption rates and a system sufficiently open to volatiles to minimize explosive disruption of the magma (Cashman, 2004). Moreover, viscosity and the effusion rate are often thought to be related to the distance reached by a lava flow; the higher the effusion rate and the lower the viscosity, the further a lava flow travels (Walker, 1973). However, in Paricutin we observed that the eruptive phases characterized by the highest effusion rates (or highest emitted volumes; e.g., 3, 19, 17,13, 4, 7,8) and with variable viscosities (Fig. 4), are not directly linked to the longest distances reached by the lava flows (e.g., 19, 17, 13); therefore, we conclude that the paleotopography might play an important role in the area covered by a single lava flow.

The cessation of the eruption could potentially be linked to intrinsic magmatic parameters. For example, the observed increase in effective viscosity could be an explanation for the abrupt termination of the Paricutin eruption. However, prior studies, including a compilation of data for pre-eruptive magma viscosities, have shown that the upper limit for viscosities of eruptible magmas rarely exceeds 10^6 Pa·s (Takeuchi, 2011). In contrast, the present study shows that all Paricutin lava flows have viscosities that fall below $2.5 \cdot 10^3$ Pa·s.

Therefore, the termination of the Paricutin eruption does not appear to be exclusively related to high effective viscosity, but rather might be a combination of limited supply of magma and progressive volatile loss, as has been proposed for other monogenetic volcanic systems (Cashman, 2004; Smith and Németh, 2017) and consistent with the overall decrease in effusion rate in the last eruptive phases (Fig. 4). Together, this would promote stalling, cooling, crystallization and an increase in density of the residual magma, which would ultimately become uneruptible.

5.3. Comparison with other monogenetic volcanoes in the MGVF

Paricutin volcano is arguably the most famous, and certainly the most thoroughly documented, among the monogenetic volcanoes that comprise the MGVF. As such, it is frequently used as a model for inferring magma characteristics and eruption parameters (e.g., volume, duration, eruption rate, etc.) of other monogenetic volcanoes in the MGVF. However, in their preliminary assessment of the MGVF, Hasenaka and Carmichael (1985) already showed decades ago that this simplistic supposition is erroneous, and that monogenetic volcanoes in this field not only display a large variety of landforms (e.g., scoria cones, maars, domes, voluminous shields, etc.) but also differ widely in composition, ranging from calc-alkaline basalts to rhyolites, including rare alkaline rocks. Furthermore, even among scoria cones alone, a great diversity of sizes, forms, and compositions can be distinguished: they occur as isolated, almost perfect cones without any associated lava flow (e.g. Juanyan, near Cherán; Siebe et al., 2014), as breached cones with horseshoe-shaped craters and hummocky debris avalanches at their base (e.g., Las Cabras near Zacapu; Siebe et al., 2014), as chains of several aligned cones formed by a single eruption (e.g., Jorullo, Guilbaud et al., 2011; Rasoazanamparany et al., 2016), or with associated single short lava flows (e.g., El Melón). Other examples display even greater differences, such as El Caracol to the NE of Zacapu, which started erupting phreatomagmatically and formed a tuff cone, before switching into a dry-magmatic Strombolian-effusive mode forming a superimposed scoria cone with associated lava flows (Kshirsagar et al., 2016). Consequently, future hazards in the MGVF are difficult to assess, as not only the location and timing, but also the physical behavior, of the next eruption are unknowable at this point. Detailed studies of a wide variety of monogenetic volcanoes occurring in the MGVF, similar to that presented here, could allow constraints to be placed on a range of possible future scenarios, including potential relationships between eruption magnitude and size and severity of affected areas. All of these depend on several variables, but most importantly on the total erupted volume, composition, and effusion rate. Any exercise of this type will necessarily have to reference Paricutin's historic eruption for comparison in terms of its eruption parameters, including volume and discharge rate of its lavas (as recalculated in this study).

If we compare the mixed violent-Strombolian/effusive eruption of Paricutin with what is known from the few other monogenetic volcanoes that have been recently studied in more detail within the MGVF, it is possible to conclude in a preliminary fashion that Paricutin's lava field covering ~25 km^2 with ~1.59–1.68 km^3 (DRE) is intermediate in terms of area covered by lavas and total erupted volume. For example, El Jorullo, the only other historic monogenetic volcano of the MGVF, covered a much smaller area (~11 km^2) with only ~0.35 km^3 (DRE) of lava flows and an overall eruption rate of 1 m^3/s (Rowland et al., 2009; Guilbaud et al., 2011), being therefore a smaller eruption in terms of volume, effusion rate, and areal extent than Paricutin. Furthermore, in the 690 km^2 Tacámbaro-Puruarán area, located at the arc-front of the MGVF, a total of 114 Quaternary volcanoes (early-Pleistocene to Holocene) were identified and mapped by Guilbaud et al. (2012). Most of these eruptions involved smaller volumes (< 0.5 km^3 DRE) than Paricutin and covered also much smaller areas with lava. In strong contrast, a much larger monogenetic eruption in the MGVF took place ~1250 CE, only ~30 km to the E of Paricutin, forming El Metate shield volcano (Chevrel et al., 2016a; Mahgoub et al., 2017a). Its voluminous lavas (9.2 km^3 DRE) cover an area of 103 km^2 and were emplaced over the course of at least 34 years, with a maximum emplacement duration of ~275 years (Chevrel et al., 2016b). Hence, it is almost six times larger in volume than Paricutin's lava field.

6. Conclusions and implications

Historic Paricutin volcano is one of the best reference examples for studying the temporal, spatial, and compositional evolution of a

monogenetic scoria cone, not only throughout its full cycle of activity, but also for the time beyond, when erosion, soil formation, and reclamation by vegetation further shape its morphology. In this context, we refined the volume estimate of lava emitted by the volcano during its 9 years of activity by combining previously published historic documentation and modern GIS and mapping tools. This new calculation, based on pre-, syn-, and post-eruption topographic maps yielded a total lava flow volume ranging between 1.59 and 1.68 km^3 (DRE), which is double the previous estimates based on simpler methods. The combined knowledge of emitted volume and geochemical composition for each lava flow throughout time will allow for better constrained petrological models, as well as inferences about the nature of the plumbing system feeding such types of eruptions.

Moreover, in this work we have presented a new geological map of the Paricutin lava field, which illustrates in a simple manner the intricate superposition of multiple partly overlapping flows. Hence, it can serve as a point of reference and guide when studying and mapping older lava fields, especially useful when several individual flows can be identified on aerial photos but are difficult to map/identify in the field.

Finally, due to the large diversity of monogenetic volcanoes comprising the MGVF, future hazard studies will have to necessarily consider multiple scenarios, involving different parameters, especially in terms of erupted lava volume, composition, and discharge rate. In this quest, the historic Paricutin eruption will play an important role, not only because it represents one of the several possible scenarios, but also because its eruption parameters (namely volume and composition) will serve as a starting point for comparing and calibrating other scenarios.

Acknowledgments

This work was supported by the National Science Foundation EAR grant #1019798 “Identifying Crustal and Mantle Processes in the Central Trans-Mexican Volcanic Belt”- awarded to Dr. E. Widom, and by Consejo Nacional de Ciencia y Tecnología (CONACyT-167231) and Dirección General de Asuntos del Personal Académico (UNAM-DGAPA IN-101915) granted to C. Siebe. We kindly thank the Department of Mineral Sciences of the Smithsonian Institution for providing us with three specimens for this study. Stimulating discussion with Laura Becerril, John Maingi and Ainhoa Lorenzo helped to develop many of the ideas presented here. Capitán Fernando Valencia is thanked for skillful and safe flight over the study area. Editor Kelly Russell is warmly thanked for comments, suggestions and editorial handling; Natalia Pardo and one anonymous reviewer are thankfully acknowledged for their constructive reviews, which led to great improvement of the manuscript.

References

Bannister, V., Roeder, P., Poustovetov, A., 1998. Chromite in the Paricutin lava flows (1943–1952). J. Volcanol. Geotherm. Res. 87, 151–171.

Bottinga, Y., Weill, D.F., 1972. The viscosity of magmatic silicate liquids: a model for calculation. Am. J. Sci. 272, 438–475.

Cashman, K.V., 2004. Volatile controls on magma ascent and eruption. In: Sparks, R.S.J., Hawkesworth, C.J. (Eds.), The State of the Planet: Frontiers and Challenges in Geophysics. American Geophysical Union, Washington, D. C https://doi.org/10.1029/150GM10.

Cebriá, J.M., Martiny, B.M., López-Ruiz, J., Morán-Zenteno, D.J., 2011. The Parícutin calc-alkaline lavas: new geochemical and petrogenetic modelling constraints on the crustal assimilation process. J. Volcanol. Geotherm. Res. 201, 113–125.

Cervantes, P., Wallace, P., 2003. Magma degassing and basaltic eruption styles: a case study of V2000 year BP Xitle volcano in central Mexico. J. Volcanol. Geotherm. Res. 120, 249–270.

Chevrel, M.O., Guilbaud, M.N., Siebe, C., 2016a. The ~AD 1250 effusive eruption of El Metate shield volcano (Michoacán, Mexico): magma source, crustal storage, eruptive dynamics, and lava rheology. Bull. Volcanol. 78:32. https://doi.org/10.1007/s00445-016-1020-9.

Chevrel, M.O., Siebe, C., Guilbaud, M.N., Salinas, S., 2016b. The AD 1250 El Metate shield volcano (Michoacán): Mexico's most voluminous Holocene eruption and its significance for archaeology and hazards. The Holocene 26 (3):471–488. https://doi.org/10.1177/0959683615609757.

Connor, C.B., Conway, F.M., 2000. Basaltic volcanic fields. In: Sigurdsson, H. (Ed.), Encyclopedia of Volcanoes. Academic Press, New-York, pp. 331–343.

Dóniz-Páez, J., De Jesús Rojas, J.C., Zamorano Orozco, J.J., Becerra-Ramírez, R., 2013. El Patrimonio geomorfológico de los volcanes de El Malpaís de Güimar (Tenerife, España) y Parícutin (Michoacán, México): implicaciones geoturísticas. In: Vegas, J., Salazar, A., Díaz-Martínez, E., Marchán, C. (Eds.), Patrimonio geológico, un recurso para el desarrollo. Cuadernos del Museo Geominero. n° 15, Instituto Geológico y Minero de España, Madrid, pp. 1–10.

Dvorak, J.J., Dzurisin, D., 1993. Variations in magma supply rate at Kilauea volcano, Hawaii. J. Geophys. Res. 98, 22255–22268.

Eggler, D.H., 1972. Water-saturated and undersaturated melting relations in a Parícutin andesite and an estimate of water content in the natural magma. Contrib. Mineral. Petrol. 34, 261–271.

Erlund, E.J., Cashman, K.V., Wallace, P.J., Pioli, L., Rosi, M., Johnson, E., Delgado Granados, H., 2010. Compositional evolution of magma from Parícutin volcano, Mexico: the tephra record. J. Volcanol. Geotherm. Res. 197, 167–187.

Fisher, R.V., Schmincke, H.U., 1984. Pyroclastic Rocks. Springer-Verlag, Berlin Heidelberg New York Tokyo (472 pp).

Foshag, W.F., 1950. The aqueous emanation from Paricutin volcano. Am. Mineral. 35, 749–755.

Foshag, W.F., González-Reyna, J., 1956. Birth and development of Parícutin volcano, Mexico. U.S. Geol. Surv. Bull. 965D, 355–485.

Fries, C., 1953. Volumes and weights of pyroclastic material, lava and water erupted by Parícutin volcano, Michoacán, Mexico. Trans. Am. Geophys. Union 34 (4), 603–616.

Genareau, K., Valentine, G.A., Moore, G., Hervig, R.L., 2010. Mechanisms for transition in eruptive style at a monogenetic scoria cone revealed by microtextural analyses (Lathrop Wells volcano, Nevada, U.S.A). Bull. Volcanol. 72, 593–607.

Guilbaud, M.N., Siebe, C., Layer, P., Salinas, S., Castro-Govea, R., Garduño-Monroy, V.H., Le Corvec, N., 2011. Geology, geochronology, and tectonic setting of the Jorullo volcano region, Michoacán, México. J. Volcanol. Geotherm. Res. 201, 97–112.

Guilbaud, M.N., Siebe, C., Layer, P., Salinas, S., 2012. Reconstruction of the volcanic history of the Tacámbaro-Puruarán area (Michoacán, México) reveal high frequency of Holocene monogenetic eruptions. Bull. Volcanol. 74, 1187–1211.

Harris, A.J.L., Dehn, J., Calvari, S., 2007. Lava effusion rate definition and measurement: a review. Bull. Volcanol. 70, 1–22.

Hasenaka, T., Carmichael, I.S.E., 1985. The cinder cones of Michoacán-Guanajuato, Central Mexico: their age, volume and distribution, and magma discharge rate. J. Volcanol. Geotherm. Res. 25, 105–124.

Inbar, M., Lugo Hubp, J., Villers Ruiz, L., 1994. The geomorphological evolution of the Paricutin cone and lava flows, Mexico, 1943–1990. Geomorphology 9, 57–76.

Kim, Y., Miller, M.S., Pearce, F., Clayton, R.W., 2012. Seismic imaging of the Cocos plate subduction zone system in central Mexico. Geochem. Geophys. Geosyst. 13 (7), Q07001.

Krauskopf, K., 1948. Mechanism of eruption at Paricutin volcano, Mexico. Geol. Soc. Am. Bull. 59, 711–731.

Krauskopf, K., Williams, H., 1946. The activity of Parícutin during its third year. Am. Geophys. Union Trans. 27:406–410. https://doi.org/10.1029/TR027i003p00406.

Kshirsagar, P., Siebe, C., Guilbaud, M.N., Salinas, S., 2016. Geological and environmental controls on the change of eruptive style (phreatomagmatic to Strombolian-effusive) of Late Pleistocene El Caracol tuff cone and its comparison with adjacent volcanoes around the Zacapu basin (Michoacán, México). J. Volcanol. Geotherm. Res. 318, 114–133.

Le Bas, M., LeMaitre, R., Strekckeisen, A., Zanettin, B., 1986. A chemical classification of volcanic rocks on the total alkali-silica diagram. J. Petrol. 27, 745–750.

Lorenzo-Merino, A., Guilbaud, M.N., Roberge, J., 2017. The violent-Strombolian eruption of 10 ka Pelado shield volcano, Sierra Chichinautzin, and implications for monogenetic hazards in the Trans-Mexican Volcanic Belt. Bull. Volcanol. (under revision).

Luhr, J.F., 2001. Glass inclusions and melt volatile contents at Parícutin Volcano, Mexico. Contrib. Mineral. Petrol. 142, 261–283.

Luhr, J.F., Simkin, T., 1993. Parícutin. The Volcano Born in a Mexican Cornfield. Geoscience Press, Phoenix (427 pp).

Mahgoub, A.N., Böhnel, H., Siebe, C., Chevrel, M.O., 2017a. Paleomagnetic study of El Metate shield volcano (Michoacán, Mexico) confirms its monogenetic nature and young age (~1250 CE). J. Volcanol. Geotherm. Res. 336, 209–218.

Mahgoub, A.N., Böhnel, H., Siebe, C., Salinas, S., Guilbaud, M.-N., 2017b. Paleomagnetically inferred ages of a cluster of Holocene monogenetic eruptions in the Tacámbaro-Puruarán área (Michoacán, México): implications for volcanic hazards. J. Volcanol. Geotherm. Res. https://doi.org/10.1016/j.jvolgeores.2017.10.004.

McBirney, A.R., Taylor, H.P., Armstrong, R.L., 1987. Paricutin re-examined: a classic example of crustal assimilation in calc-alkaline magma. Contrib. Mineral. Petrol. 95, 4–20.

Németh, K., Carrasco-Nuñez, G., Aranda-Gómez, J.J., Smith, I.E.M. (Eds.), 2017. Monogenetic Volcanism. Geological Society, London (Special Publications, 446).

Parfitt, E.A., Wilson, L., 1995. Explosive volcanic eruptions—IX. The transition between Hawaiian-style lava fountaining and Strombolian explosive activity. Geophys. J. Int. 121 (1), 226–232.

Pérez-Vega, A., François-Mas, J., 2009. Evaluación de los errores de modelos digitales de elevación obtenidos por cuatro métodos de interpolación. Investig. Geogr. 69, 53–79.

Pioli, L., Erlund, E., Johnson, E., Cashman, K., Wallace, P., Rosi, M., Delgado Granados, H., 2008. Explosive dynamics of violent Strombolian eruptions: the eruption of Parícutin Volcano 1943–1952 (Mexico). Earth Planet. Sci. Lett. 271, 359–368.

Pyle, D.M., Elliot, J.R., 2006. Quantitative morphology, recent evolution, and future activity of the Kameni Islands volcano, Santorini, Greece. Geosphere 2, 253–268.

Rasoazanamparany, C., Widom, E., Siebe, C., Guilbaud, M.N., Spicuzza, M.J., Valley, J.W., Valdez, G., Salinas, S., 2016. Temporal and compositional evolution of Jorullo volcano, Mexico: implications for magmatic processes associated with a monogenetic eruption. Chem. Geol. 434, 62–80.

Rodriguez-Gonzalez, A., Fernandez-Turiel, J.L., Perez-Torrado, F.J., Gimeno, D., Aulinas, M., 2010. Geomorphological reconstruction and morphometric modelling applied to past volcanism. Int. J. Earth Sci. 99, 645–660.

Rowe, M.C., Peate, D.W., Ukstins Peate, I., 2011. An investigation into the nature of the magmatic plumbing system at Paricutin volcano, Mexico. J. Petrol. 52 (11), 2187–2220.

Rowland, S.K., Harris, A.J.L., Wooster, M.J., Amelung, F., Garbeil, H., Wilson, L., Mouginis-Mark, P.J., 2003. Volumetric characteriscs of lava flow from interferometric radar and multispectral satellite data: the 1995 Fernandina and 1998 Cerro Azul eruptions in the western Galapagos. Bull. Volcanol. 65, 311–330.

Rowland, S.K., Jurado-Chichay, Z., Ernst, G., Walker, G.P.L., 2009. Pyroclastic deposits and lava flows from the 1759–1774 eruption of El Jorullo, México: Aspects of "Violent Strombolian" activity and comparison with Paricutin. In: Thordarson, T., Self, S., Larsen, G., Rowland, S.K., Hoskuldsson, A. (Eds.), Studies in Volcanology: The Legacy of George Walker: Geol. Soc. London Spec. Publ. 2, pp. 105–128.

Scandone, R., 1979. Effusion rate and energy balance of Paricutin eruption (1943–1952), Michoacan, Mexico. J. Volcanol. Geotherm. Res. 6, 49–59.

Segerstrom, K., 1950. Erosion studies at Parícutin, State of Michoacán, Mexico. U.S. Geol. Surv. Bull. 965A, 1–164.

Siebe, C., Guilbaud, M.N., Salinas, S., Kshirsagar, P., Chevrel, M.O., de la Fuente, J.R., Hernández-Jiménez, A., Godínez, L., 2014. Monogenetic Volcanism of the Michoacán-Guanajuato Volcanic Field: Maar Craters of the Zacapu Basin and Domes, Shields, and Scoria Cones of the Tarascan Highlands (Paracho-Paricutin Region). Fieldguide, Pre-meeting Fieldtrip (Nov. 13–17) for the 5th International Maar Conference (5IMC-IAVCEI), Querétaro, México (33 p).

Smith, I.E.M., Németh, K., 2017. Source to surface model of monogenetic volcanism: a critical review. Geol. Soc. Lond., Spec. Publ. 446, 1–28.

Takeuchi, S., 2011. Preeruptive magma viscosity: an important measure of magma eruptibility. J. Geophys. Res. Solid Earth 116 (B10). https://doi.org/10.1029/2011JB008243.

Tucker, G.E., Lancaster, S.T., Gasparini, N.M., Braas, R.L., Rybarczyk, S.M., 2001. An object-oriented framework for distributed hydrologic and geomorphic modeling using triangulated irregular networks. Comput. Geosci. 21, 959–973.

Valentine, G.A., Connor, C.B., 2015. Basaltic volcanic fields. In: Sigurdsson, H., Houghton, B.F., McNutt, S.R., Rymer, H., Stix, J. (Eds.), Encyclopedia of Volcanoes, 2nd edn. Academic Press, London, pp. 423–439.

Walker, G.P.L., 1973. Lengths of lava flows. Phil. Trans. R. Soc. Lond. A. 274, 107–118.

Wilcox, R.E., 1950. Volcanoes of the Parícutin Region, Mexico. U.S. Geol. Surv. Bull. 965B, 165–280.

Williams, H., 1950. Petrology of Parícutin volcano, Mexico. U.S. Geol. Surv. Bull. 965C, 281–354.

Yokoyama, I., De la Cruz-Reyna, S., 1990. Precursory earthquakes of the 1943 eruption of Paricutin volcano, Michoacan, Mexico. J. Volcanol. Geotherm. Res. 44 (3–4), 265–281.